VOL. 21, NO. 1, 2022, 25-34
www.fke.utm.my/elektrika
ISSN 0128-4428

ELEKTRIKA
Journal of Electrical Engineering

The Logarithmically-non-uniform Helix Antenna Mounted Above a Finite Ground Plane

Ike Mowete[1*], Ayotunde Ayorinde[1] and **Adeniyi Adehola[2]**

[1]University of Lagos, Akoka, Lagos, Nigeria
[2]Federal University, Otuoke, Bayelsa State, Nigeria

[*]Corresponding author: amowete@unilag.edu.ng

Abstract: In this paper the influence of ground plane size on the performance characteristics of a thin-wire helical antenna characterized by a logarithmically varying turns spacing, and mounted above a circular ground plane of finite extent, is systematically investigated. The moment-method formulation utilized in the paper involves a wire-grid model for the ground plane as well as explicit expressions, deriving from a vector potential approach, for the radiation fields of this 'loghelix'. Subsequent computational results obtained for a candidate 8-turn 'loghelix' axial-mode $\left(0.8 \le C_{\lambda} \le 1.4\right)$ antenna using various combinations of 'logarithmic variation factor' and ground plane size, very clearly reveal that limiting the size of the ground plane to finite dimensions significantly improves antenna performance. Maximum gain obtainable, for example, emerged as 16.45dBi when a finite ground plane is utilized, as against 13.55dBi for the corresponding antenna, backed by an infinite ground plane. The associated axial ratio performance is characterized by $0.44\text{dB} \le \text{average axial ratio} \le 1.22\text{dB}$ for the finite ground case, and $1.96\text{dB} \le \text{average axial ratio} \le 2.75\text{dB}$, for the infinite ground plane case. A notable finding of the investigations is that the dip that typically features in the power gain profiles of antenna structures backed by finite ground planes will be eliminated, when ground plane size, relative to antenna size exceeds a certain minimum.

Keywords: Axial mode, finite ground plane, helical antenna, logarithmic turns spacing, wire-grid

Article History: received 1 December 2021; accepted 28 March 2022; published 20 April 2022.

1. INTRODUCTION

In one of the earliest rigorous investigations of the effects of size on antenna performance, Harrington [1], demonstrated that optimum gain, efficiency, and bandwidth achievable are functions of the device's physical size, measured in units of wavelength. Since then, quite a few other size-based investigations, many of them with focus on the influence of the size of the finite ground plane in the antenna structure, have been reported in the open literature. Notable examples of these include contributions described in [2] and [3], for the rectangular microstrip antenna, [4], for the microstrip-fed monopole, and in [5] and [6], for the circular loop antenna. Others are the contributions of Bolli et al [7], concerning the aperture array of log-periodic antennas deployed for Earth station use in the SKA1-Low radio telescope: and the treatment of finite-ground-plane-backed monopole, reported by Basaery et al, [8].

For the helical antenna, which is the focus of this paper, several research publications ([9], [10], for example) have firmly established that size and shape of the finite ground plane have significant consequences for the antenna's gain, axial-ratio bandwidth, and input impedance responses. Contributions by Nakano et al [**10**] revealed that for the uniformly wound helix, conventional axial mode operation is maintained if the diameter of a backing finite circular conductor is at least 0.6λ at the operating frequency; and that if the size of the diameter is reduced to 0.4λ, a 'backfire' axial mode operation results. According to the results reported by Ahmad et al, [**11**], for the Quadrifilar Helical Antenna (QHA), the antenna's input impedance remains virtually constant, if its height above a finite ground plane is at least 0.3λ. As a matter of fact, a related contribution in [12] optimized the far-zone radiation characteristics of the QHA through an informed prescription of finite ground plane size. Results presented in the paper suggested that whereas the QHA backed by finite ground planes generally provided better (compared to infinite ground plane) 3dB axial ratio bandwidth and boresight axial ratio, in Low-Earth Orbit satellites, however, stability in input and far-zone parameters is achievable at the expense degraded boresight axial ratio. Wadkar et al [13], investigated the influence of a small circular ground plane on the performance parameters of a uniformly wound, axial-mode antenna, to find that a maximum gain of 2.08dB is obtained when the radius of the ground plane is $\lambda/30$, for a wire radius of $\lambda/100$. Sadeghikia and Horestam [14] reported a somewhat similar situation for a uniformly wound helical antenna operated in the axial mode, and utilized for space communications. The two key findings reported in [14] are that antenna optimum performance is

achieved when ratio of ground-plane radius to helix radius is 1.5, and for this ratio, performance is independent of number of helical turns.

A number of publications have suggested that the introduction of some non-uniformity into the geometry of the axial mode helical antenna represents a means of enhancing performance. Egorov and Ying [15], for example, described how the introduction of a geometrical non-uniformity may be utilized for the excitation of two distinct resonant frequencies by the helical antenna, for dual mode mobile telephony applications. Elkamchouchi and Salem, [16], [17], who investigated the effects of two types (exponential and logarithmic variation of helix diameter) of geometrical non-uniformities, reported comparative outcomes, which suggested that the introduction of both the logarithmic and exponential variations in helix diameter attracted improvements in all antenna performance metrics over the uniformly wound helix. Further improvements were recorded for the best performing 'exponential helix, [17], when a ground plane was introduced into the structure, with what the authors referred to as "a noticeable improvement in gain". The conclusions in [16] and [17] concerning the exponential helix are supported by the results presented by Chen et al [18], who considered an exponentially varying turns spacing, for which axial-ratio bandwidth improved by close to 59% over that for an equivalent linearly spaced helix. It may be remarked in that connection that whereas [17] utilized a large (infinite) ground plane, the square ground plane utilized in [18] had finite dimensions.

Because a recent publication by Ayorinde et al [19], suggest that the helical antenna characterized by a logarithmic non-uniformity in its turns spacing, has better performance metrics than the 'exponential helix' of about the same geometrical profile, and since, as noted by Nakano et al [10], a finite ground plane significantly improves the helical antenna's gain and axial ratio performances, this paper is motivated to examine the influence of ground plane size on the performance of the 'loghelix'.

Using the same 8-turns axial mode helical antenna treated in [19] for the purposes of comparative evaluation, the paper presents a method-of-moments investigation, in which the finite ground plane is modeled as a wire grid of the type described in [6], [10], [20]. The computational results due to the analytical model very clearly demonstrate that the logarithmically non-uniform helical antenna's performance improves remarkably, when the structure's ground plane is of finite extent. In particular, over the frequency range considered, maximum achievable gain improved by about 3dBi (or 21.4%) whilst average axial ratio attracted close to a 58% increase.

A notable outcome of the study is that the power gain profiles associated with wire antenna structures backed by finite ground planes need not exhibit dips of the type suggested by the results of [5], [6], and [23], as being characteristic of such antennas. For the relevant results obtained in this paper reveal (for the first time, to the best of our knowledge) that when the size of the ground plane relative to that of the antenna ('aspect ratio') exceeds a certain minimum, the said dips will be eliminated.

.

2. ANALYSIS

The geometry of Figure 1 describes a general N-turn helical antenna of circular cross section whose turns spacing varies logarithmically along its axis, and which is mounted on a circularly-shaped ground plane of finite extent.

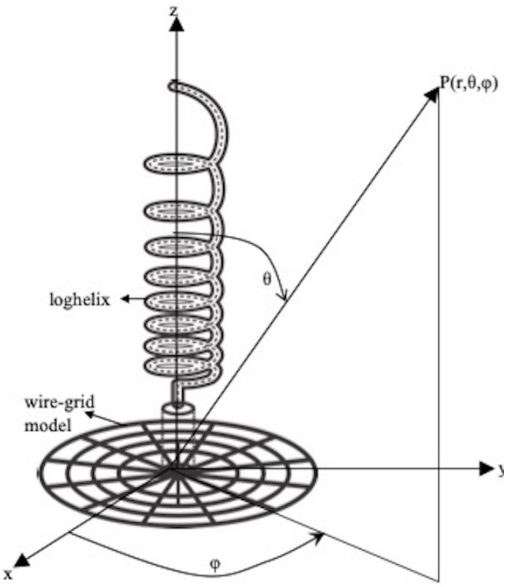

Figure 1. Problem Geometry

Because the ground plane is modeled by a wire-grid consisting of circular-loop and radial elements, the vector magnetic potential for the problem admits description as a superposition of three contributing components: one due to the 'loghelix', and the other two, due to radial and circular-loop components, respectively, of the wire grid.

For the loghelix, and following developments fully described in **[19]**, it is readily established that the Cartesian components of the vector potential are given by

$$A_x = \frac{-a\mu_0 e^{-jk_0 r}}{4\pi r}\int_0^{2\pi N} \sin\phi' I(\phi') e^{jk_0 a[\sin\theta\cos(\varphi-\phi')+\xi\cos\theta]} d\phi' \tag{1a}$$

$$A_y = \frac{a\mu_0 e^{-jk_0 r}}{4\pi r}\int_0^{2\pi N} \cos\phi' I(\phi') e^{jk_0 a[\sin\theta\cos(\varphi-\nu)+\xi\cos\theta]} d\phi' \tag{1b}$$

and

$$A_z = \left(\frac{a\mu_0 e^{-jk_0 r}}{4\pi r}\right)\left(\frac{2\pi N\beta\tan\alpha}{\ln\Phi_N}\right)\int_0^{2\pi N}\frac{1}{\Phi_N-\beta\phi'} I(\phi') e^{jk_0 a[\sin\theta\cos(\varphi-\phi')+\xi\cos\theta]} d\phi \tag{1c}$$

provided that the symbol ξ, which features in the phase terms of the foregoing equations is defined by

$$\xi = \left(\frac{2\pi N\tan\alpha}{\ln\Phi_N}\right)\left(\ln\left[\frac{\Phi_N}{\Phi_N-\beta\phi'}\right]\right) \tag{1d}$$

It is also to be noted that for these expressions, 'a' stands for the radius of loghelix, ϕ' a 'source quantity'- a running variable along the turns of the helix; whilst β represents the structure's 'logarithmic variation factor', and Φ_N, which in part, defines this factor, is given by

$\Phi_N = 2\pi N\beta + 1$; with α representing helix pitch angle of the originally uniform helix.

Vector magnetic potential for the mth circular-loop element of the wire grid has the Cartesian components identified as

$$A_x = \frac{-\mu_0 a_m e^{-jk_0 r}}{4\pi r}\int_0^{2\pi} \sin\varphi' I(\varphi') e^{jk_o a_m \sin\theta\cos(\varphi-\varphi')} d\varphi' \quad (2a)$$

and

$$A_y = \frac{\mu_0 a_m e^{-jk_0 r}}{4\pi r}\int_0^{2\pi} \cos\varphi' I(\varphi') e^{jk_o a_m \sin\theta\cos(\varphi-\varphi')} d\varphi' \quad (2b)$$

whilst for the linear elements of the wire-grid, each of length symbolized by L_r, vector potential's Cartesian components are readily evaluated as

$$A_x = \frac{\mu_0 e^{-jk_0 r}\cos\varphi'_n}{4\pi r}\int_{L_r} I(l') e^{jk_0 l'\sin\theta\cos(\varphi-\varphi'_n)} dl' \quad (3a)$$

in which φ_n identifies the inclination of nth radial element to the x-axis.

Finally,

$$A_y = \frac{\mu_0 e^{-jk_0 r}\sin\varphi'_n}{4\pi r}\int_{L_r} I(l') e^{jk_0 l'\sin\theta\cos(\varphi-\varphi'_n)} dl' \quad (3b)$$

The angular measure denoted by ϕ in Equations (1a) - (1c) is a running variable associated with the geometry of the loghelix, and should not be confused with φ', a spherical coordinate variable. And for Equations (3a) and (3b),

$$\varphi_n = \frac{2\pi}{V}(n-1), \quad n = 1, 2, \ldots, V \quad (3c)$$

When the well-known radiation-zone approximation characterized by $\mathbf{E} = -j\omega\mathbf{A}$ is utilized, and upon invoking the usual Cartesian-to-Spherical coordinates transformation, the radiation field integrals associated with the vector magnetic potentials defined by Equations (1) – (3) readily emerge as follows:

$$E_\theta^{hel} = \frac{-j\omega\mu_0 a e^{-jk_0 r}}{4\pi r}\int_0^{2\pi N}\left[\begin{array}{l}\left(\cos\theta\sin(\varphi-\phi') - \dfrac{2\pi N\beta\tan\alpha\cos\varphi}{(\Phi_N-\beta\phi')\ln\Phi_N}\right)\times \\ \times\left(I(\phi') e^{jk_0 a[\sin\theta\cos(\varphi-\phi')+\xi\cos\theta]}\right)\end{array}\right] d\phi' \quad (4a)$$

and

$$E_\varphi^{hel} = \frac{-j\omega\mu_0 a e^{-jk_0 r}}{4\pi r}\int_0^{2\pi N}\left(\cos(\varphi-\phi')\right)\left(I(\phi') e^{jk_0 a[\sin\theta\cos(\varphi-\phi')+\xi\cos\theta]}\right) d\phi' \quad (4b)$$

being the contributions from the loghelix, with

$$E_\theta^{cir} = \frac{-j\omega\mu_0 a_m e^{-jk_0 r}\cos\vartheta}{4\pi r}\int_0^{2\pi}\sin(\varphi-\varphi') I(\varphi') e^{jk_0 a_m \sin\theta\cos(\varphi-\varphi')} d\varphi' \quad (5a)$$

$$E_\varphi^{cir} = \frac{-j\omega\mu_0 a_m e^{-jk_0 r}}{4\pi r}\int_0^{2\pi}\cos(\varphi-\varphi') I(\varphi') e^{jk_0 a_m \sin\theta\cos(\varphi-\varphi')} d\varphi' \quad (5b)$$

as contribution from each circular-loop element of the wire-grid. Contributions from each of the radial elements of the wire-grid are

$$E_\vartheta^{rdl} = \frac{-j\omega\mu_0\cos\vartheta\cos(\varphi-\varphi'_n) e^{-jk_0 r}}{4\pi r}\int_{L_m} I(l') e^{jk_0 l'\sin\theta\cos(\varphi-\varphi_n)} dl' \quad (6a)$$

and

$$E_\varphi^{rdl} = \frac{-j\omega\mu_0\sin(\varphi'_n-\varphi) e^{-jk_0 r}}{4\pi r}\int_{L_m} I(l') e^{jk_0 l'\sin\theta\cos(\varphi-\varphi'_n)} dl' \quad (6b)$$

2.1 Moment-method solution

The solution to the problem formulated by the analysis presented in the foregoing discussions requires the determination of the only unknown (current distribution) quantity appearing in Equations (4) to (6). In this paper, use is made of the method of moments **[21]**, for the determination of this unknown, in the following manner.

First, expansion functions (denoted by 'T') and weighting functions (symbolized by 'W') are defined for the three (loghelix, radial, and circular-loop) thin-wire component parts of the problem geometry, and then, the generalized impedance matrix appropriate to the problem is specified according to

$$[Z] = \begin{bmatrix} \langle W_{qh}, L_h(T_{ph})\rangle & \langle W_{qh}, L_c(T_{pc}^m)\rangle & \langle W_{qh}, L_r(T_{pr}^n)\rangle \\ \langle W_{qc}, L_h(T_{ph})\rangle & \langle W_{qc}, L_c(T_{pc}^m)\rangle & \langle W_{qc}, L_r(T_{pr}^n)\rangle \\ \langle W_{qr}, L_h(T_{ph})\rangle & \langle W_{qr}, L_c(T_{pc}^m)\rangle & \langle W_{qr}, L_r(T_{pr}^n)\rangle \end{bmatrix} \quad (7)$$

The subscripts 'qh', 'qc', and 'qr' appearing in Equation (7) identify the qth weighting function defined for the geometry of the loghelix, circular-loop, and radial elements of the structure, respectively; and a similar interpretation obtains for the subscripts 'ph', 'pv', and 'pr' associated with the expansion functions. On the other hand, the superscripts 'm' and 'n' in the equation refer to the mth and nth circular-loop and radial elements of the wire-grid. 'L_p', 'L_c', and 'L_r' are linear operators **[21]**, defined with the uses of Equations (4) to (6), for loghelix, circular-loop, and radial geometries, respectively. Inner product prescribed by $\langle\bullet,\bullet\rangle$ in Equation (7) involves the use of the unit vectors, easily derived as

$$\hat{\mathbf{a}}_{hel} = \frac{-\sin\phi'\hat{\mathbf{a}}_x + \cos\phi'\hat{\mathbf{a}}_y + \left[(2\pi N\beta\tan\alpha)/(\Phi_N-\beta\phi')\ln\Phi_N\right]\hat{\mathbf{a}}_z}{\sqrt{1+\left[(2\pi N\beta\tan\alpha)/(\Phi_N-\beta\phi')\ln\Phi_N\right]^2}} \quad (8a)$$

for the loghelix, **[19]**,

$$\hat{\mathbf{a}}_{cir} = -\sin\varphi'\hat{\mathbf{a}}_x + \cos\varphi'\hat{\mathbf{a}}_y \quad (8b)$$

in the case of each circular-loop element, and

$$\hat{\mathbf{a}}_{rdl} = \cos\varphi_n\hat{\mathbf{a}}_x + \sin\varphi'_n\hat{\mathbf{a}}_y, \quad (8c)$$

for the nth radial element.

Once a voltage excitation column vector is determined for the problem, the desired current distribution becomes available through the simple matrix processes of inversion and multiplication, as explained elsewhere, [**21**].

2.1.1. Specifications

For the purposes of computational results, the dimensional and operational specifications displayed in Table 1 are utilized in the paper. Because the axial-mode loghelix backed by an infinite ground plane treated in [19] is used for comparative evaluation, this paper adopts the same frequency range of $1.6GHz \le f \le 2.8GHz$, which

corresponds to the log-helix dimensions defined by $0.8 \le C_{\lambda} \le 1.4$. The logarithmic variation factor remains the same as in [19], and the height of the antenna above the ground plane is maintained at 0.15 λ at all the frequencies considered.

Table 1. Physical specifications of antenna structure

Freq. (GHz)	C_{λ}	r_g/λ γ=3	r_g/λ γ=3.5	r_g/λ γ=4	r_g/λ) γ=4.5	r_g/λ γ=5	r_g/λ γ=6
1.6	0.8	0.381	0.445	0.508	0.572	0.635	0.762
1.8	0.9	0.429	0.501	0.572	0.644	0.715	0.858
2.0	1.0	0.477	0.557	0.636	0.716	0.795	0.954
2.2	1.1	0.525	0.613	0.700	0.788	0.875	1.050
2.3	1.15	0.549	0.641	0.732	0.824	0.915	1.098
2.4	1.2	0.573	0.669	0.764	0.860	0.955	1.146
2.5	1.25	0.597	0.697	0.796	0.896	0.995	1.194
2.6	1.3	0.621	0.725	0.828	0.932	1.035	1.242
2.8	1.4	0.669	0.781	0.892	1.004	1.115	1.338

Finite circular ground plane size is specified by an 'aspect ratio' defined by

$$\gamma = \frac{circumference\,of\ ground\ plane}{circumference\,of \log helix}, \qquad (9)$$

which, in this paper, varies between 3.0 and 6.0, as shown in Table 1. For these dimensions, Table 1 also displays the corresponding variations in ground plane radius, as frequency varies.

The computational implementation of the Method-of-Moments scheme involved a wire-grid ground plane with 4 circular loops and 12 radial elements. And in the Garlerkin approach (identical expansion and weighting functions), 64, 48, and 18 expansion functions were utilized for the loghelix, and the circular loop, and the radial elements, respectively. The computational results obtained with the use of a 1V delta-gap feed model are presented and comprehensively discussed in section 3, which follows.

3. DISCUSSION OF RESULTS

Representative computational results describing the performance of loghelix antenna backed by a finite-sized ground plane are presented in this section, starting in the next sub-section, with current distribution.

3.1. Current distribution

The current distribution profiles displayed in Figures 2.1 – 2.5 are for various values of ground plane aspect ratio, for given values of β, in the representative cases of $0.8 \le C_{\lambda} \le 1.2$

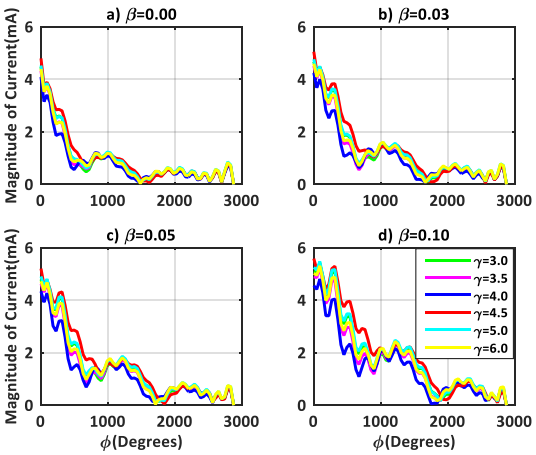

Figure 2.1. Profiles of current distribution along the helical arm length for $C_{\lambda} = 0.8$

The distributions of current along the helical arm length displayed by Figure 2.1 for C_{λ} = 0.8 reveals that regardless of the value of γ when β = 0, the decaying component and the surface wave part of the current waveforms are (with the notable exception of the case γ = 4.5) about equally divided over the helical arm length, with slight differences in profiles and magnitude distributions. The ripples on the surface-wave part of the current distributions may be directly attributed to reflections from the open end of the helical structure. When β = 0.03, the decaying segments of the current profiles now approximately occupy the first five turns of the helix, leaving the last three turns to the surface wave portion. Again, it is observed that the magnitude of current for the case γ = 4.5 is dominant especially in the decaying region. Compared to the case of β = 0, the feed-point current values are larger and the reflection from the open end of the helix have diminished slightly.

The profiles of Figures 2.1(c) and (d) for β = 0.05 and 0.1, respectively, indicate that the decaying segments of the magnitude of currents move moderately towards the open end of the helix as β increases, consequently reducing the span of the surface wave segments in comparison.

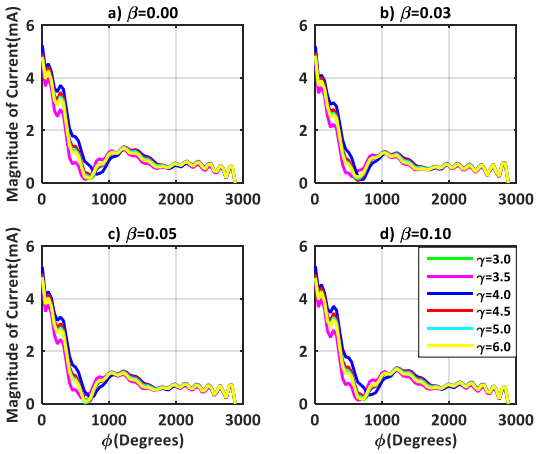

Figure 2.2.Profiles of current distribution along the helical am length for $C_{\lambda} = 0.9$

It can also be observed from the profiles that magnitude of current generally increases as the logarithmic variation factor (β) increases.

The profiles displayed in Figure 2.2 are for $C_\lambda = 0.9$, covering all the four values of β indicated. Unlike what obtained with the cases described for Figure 2.1, the decaying exponential components of magnitude of current, for various values of γ, though slightly larger, now extend only over the first two turns from the feed-point. This means that in this case, the surface wave region of the current, which, as noted in **[10]** is essentially responsible for radiation in the axial direction, now extends over the remaining six turns of the loghelix, for all sizes of ground plane considered. In this case, the extreme point of the exponentially-decaying segment of the profiles gradually moves towards the second turn as β increases. According to these distributions, reflections from the antenna's open end have significantly reduced, as evident from the mild ripples displayed by the current waveforms. This suggests that the increase in ground plane size is more influential on the exponential-decaying component of magnitude of current distribution.

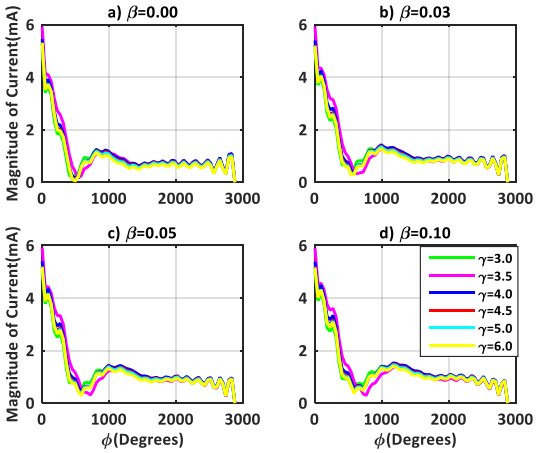

Figure 2.3.Profiles of current distribution along the helical arm length for $C_\lambda = 1.0$

The trend displayed by the profiles of Figure 2.3 (C_λ = 1.0) clearly show that the surface wave region of magnitude of current now strictly extends from about 1½ turns of the helix to the open end, for all values of aspect ratio. Compared to the profiles of Figure 2.2, magnitude of current in this case, is noticeably larger, and the influence of the logarithmic variation factor is also more pronounced. With the exception of γ = 3.5, all waveforms for other values of aspect ratio values share similar profiles. Indeed, when γ is greater than 4.0, the distributions of current magnitude for all values of β are practically identical with moderate reflections from the open end. On the other hand, for γ less than or equal to 4.0, the differences in the profiles are limited to the exponentially-decaying region located between the feed-point and about 1½ turns of the helix.

When the size of the log-helix is defined by $C_{\lambda = 1.1,}$ a distinguishing feature, as can be seen from Figure 2.4 is that the magnitude of current distribution is largest for γ = 3.5, over all values of β. And although magnitude of current is generally higher in this case than recorded for for the C_λ = 1.0 case, the exponential decaying segment current distribution for the former is still limited to the span of the arm length extending from feed-point ($\phi' = 0^o$) to 1½ turns of the helix, as with the latter.

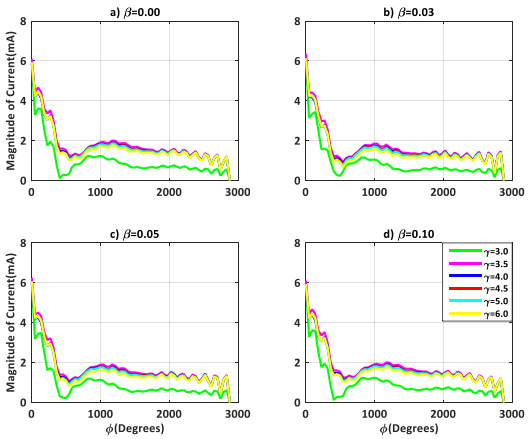

Figure 2.4.Profiles of current distribution along the helical am length for $C_\lambda = 1.1$

In comparison with the current profile when C_λ = 1.0, the current plots for C_λ = 1.1 reflect stronger reflections from the open end in view of more visible ripples especially near the open end.

For the remaining values of C_λ considered (1.2, 1.3, and 1.4) the requirement of the same vertical span for both the uniform and non-uniform geometries of the helix implies that at the end close to the feed point, the turns compression of loghelix increases significantly. The consequences of this observation for magnitude of current distribution are typified by profiles displayed in Figure 2.5, from which it can be deduced that there is significant

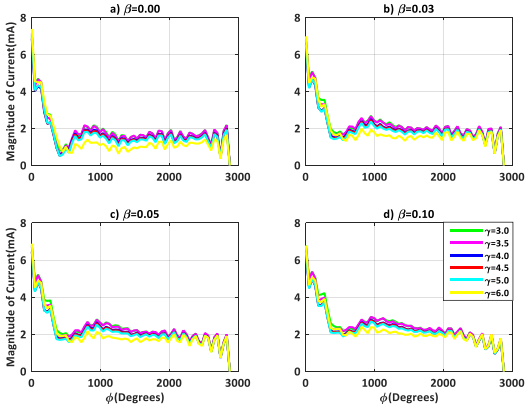

Figure 2.5.Profiles of current distribution along the helical am length for $C_\lambda = 1.2$

reflections from the antenna's open end. Other interesting features of these profiles concern the surface component of magnitude of current, for which, in this case, minimum value is recorded when aspect ratio is 6.0, for all values of β. Also, magnitude of current is largest over the span of the antenna's arm length when aspect ratio equals 3.5, again, for all values of β.

3.2. Radiation Fields

The $\hat{\mathbf{a}}_\theta$-component, in the XZ-plane, of the radiation fields corresponding the current distributions of Figure 2.1 are displayed in Figure 3.1.

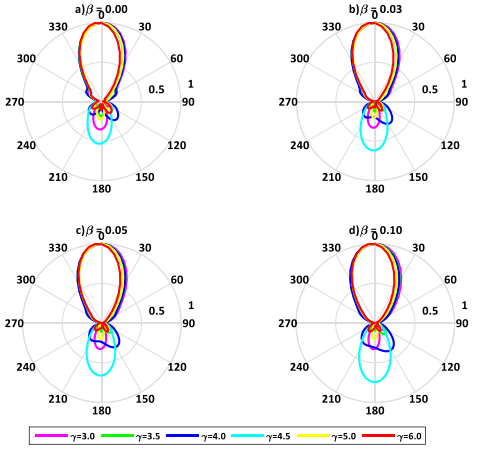

Figure 3.1. Far-zone $E_\theta(\theta,0)$ for $C_\lambda = 0.8$

It is readily observed from the profiles that the main lobes, for all values of logarithmic variation factor and aspect ratio, are completely symmetrical about the helical axis ($\theta = 0^o$) above the finite ground plane, whereas, (with the exception of $\gamma = 4.5$) the minor lobes in the backward direction ($\theta = 180^o$) below the ground plane are of relatively moderate strength. According to these profiles., the most directive beam in the forward direction ($\theta = 0^o$) is obtained in all cases of non-uniformity. When $\gamma = 4.5$, in the region above the finite ground plane modeled by wire-grids, the patterns essentially display no sidelobes, though in the backfire direction ($\theta = 180^o$), the pattern strength increases as β increases particularly for $\gamma = 4.5$ case.

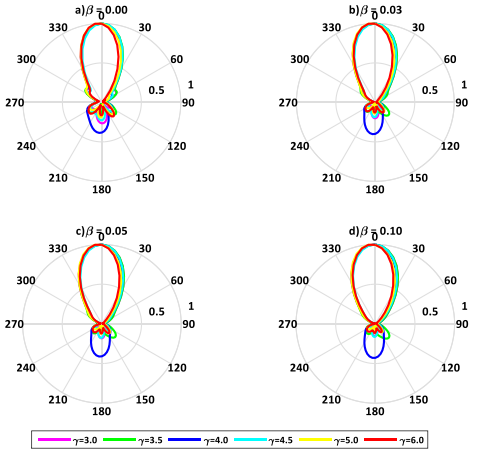

Figure 3.2. Far-zone $E_\theta(\theta,0)$ for $C_\lambda = 0.9$

Although the theta-component of the radiation field patterns corresponding to the current distribution profiles of Figure 2.2 (for $C_\lambda = 0.9$) follow the same general trend as those of Figure 3.1, one obvious difference seen from Figure 3.2 is that the most prominent back lobe is now associated with the ground plane size defined by $\gamma = 4.0$. In addition, the minor lobes in this case are of relatively lower strength, and the patterns better support the suggestion that compared with the uniform helix in terms of minor lobes below the ground plane, the loghelix is a more efficient radiator.

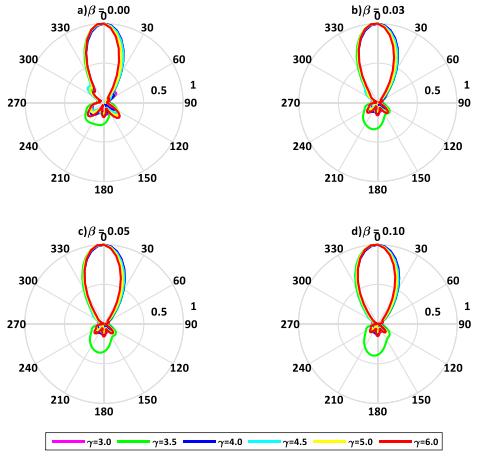

Figure 3.3. Far-zone $E_\theta(\theta,0)$ for $C_\lambda = 1.0$

Radiation field patterns for the case $C_\lambda = 1.0$ (due to the current distributions of Figure 2.3) are displayed in Figure 3.3. These patterns very clearly reveal notable improvements in both directivity of the main lobes and minor lobes of the loghelix, compared with the two cases discussed. An interesting feature of the patterns is that with the exceptions of the ground plane size cases for which $\gamma = 3.5$ *and* $\gamma = 4.0$, the patterns are virtually identical, for all degrees of non-uniformity considered. It is also interesting to observe that the back lobe strengths have decreased significantly compared to the previous cases, and the dominant back lobe, which increases in strength as β increases, is now associated with $\gamma = 3.5$.

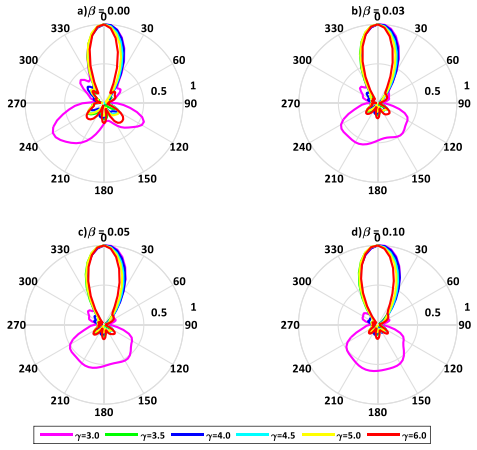

Figure 3.4. Far-zone $E_\theta(\theta,0)$ for $C_\lambda = 1.1$

At the frequency of operation for which $C_\lambda = 1.1$, the theta-component of the antenna's radiation field patterns for the different combinations of γ and β, differ significantly from those for the three values of C_λ earlier discussed, as can be seen from Figure 3.4. First, the 'dominant' back lobe characteristic of the patterns for $C_\lambda < 1.1$ has now shifted its occurrence to the ground plane defined by $\gamma = 3.0$; and is now relatively larger in strength and exhibits a considerably more pronounced degree of asymmetry. The minor lobes below the ground

plane are also relatively smaller in size, and as a matter of fact, the only noticeable side lobe above the ground plane is that associated with the $\gamma = 3.0$ patterns.

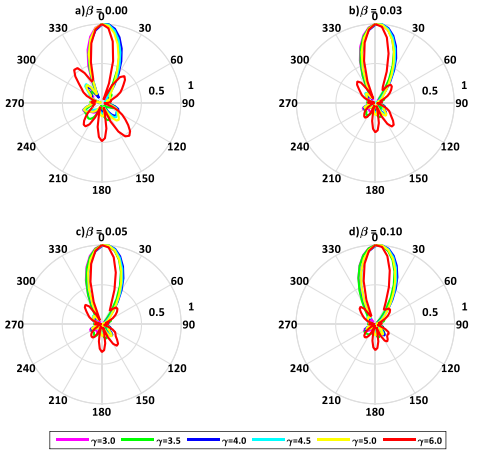

Figure 3.5. Far-zone $E_\theta(\theta,0)$ for $C_\lambda = 1.2$

Figure 3.5 displays the far-zone patterns due the current distributions of Figure 2.5, for which C_λ is 1.2. One immediately noticeable feature of the patterns is that the 'dominant backlobe' associated with patterns for the other values of C_λ earlier discussed, is not featured in this case. In addition the patterns are now characterized by sidelobes of strength relatively larger compared with those of the patterns earlier discussed; and the field patterns in the forward direction, in the case of $\gamma = 6.0$ now has a slight asymmetry.

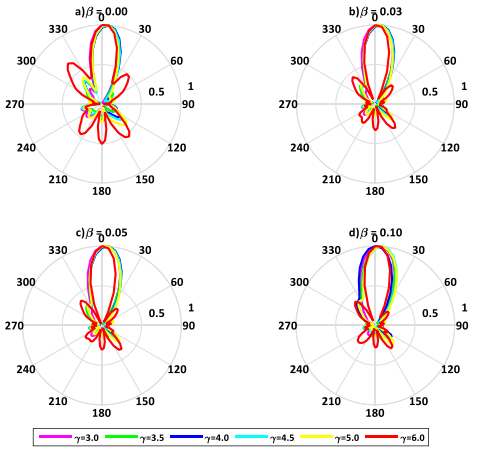

Figure 3.6. Far-zone $E_\theta(\theta,0)$ for $C_\lambda = 1.3$

Figure 3.6 reveals that with further increases in C_λ to 1.3 the slight asymmetry observed in Figure 3.5 for the patterns for $\gamma = 6.0$ become more noticeable as β increases, and extend to the other patterns. . It is further revealed that the symmetry displayed by the main lobes of field patterns for values of $C_\lambda \le 1.2$ no longer feature. And it can also be observed that significant side lobes exist, mainly below the finite ground plane, and with strengths, generally noticeably smaller than those of the corresponding patterns for $C_\lambda < 1.3$.

As confirmed by the excellent values of axial ratio (in §3.2) due to antenna for all values of ground plane size over the entire range of frequencies considered, the patterns of the φ -components of the far-zone fields are practically identical to those of the θ-components.

3.2. Axial ratio

In antenna theory and practice, Axial Ratio (AR) represents a measure of the degree of circular polarization, ascribable to an antenna's radiation field, **[22]**. For the computational results presented and described in the ensuing discussions, use is made of the expression given as **[19]**,

$$AR(dB) = 10\log_{10}\sqrt{\left[\frac{|E_\theta|^2+|E_\varphi|^2+\left(|E_\theta|^4+|E_\varphi|^4+2|E_\theta|^2|E_\varphi|^2\cos 2\delta\right)^{1/2}}{|E_\theta|^2+|E_\varphi|^2-\left(|E_\theta|^4+|E_\varphi|^4+2|E_\theta|^2|E_\varphi|^2\cos 2\delta\right)^{1/2}}\right]} \quad (10)$$

The axial ratio profiles displayed in Figure 4 describe the influence of ground plane size on the axial ratio of the logarithmically-wound helical antennas by comparing axial ratio performances of different ground plane sizes, including the infinite ground plane.

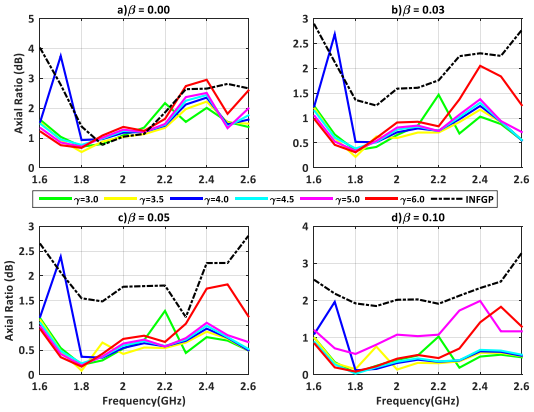

Figure 4. Axial-ratio profiles for different sizes of ground plane for various values of β

It is immediately obvious from the profiles, that the use of finite sizes for the ground plane significantly enhances the circular polarization attributes of the logarithmically wound helix. According to the results, for the uniformly wound helix, the influence of ground plane size is slight, particularly in the frequency range $1.9GHz \le f \le 2.3GHz$. With the introduction of the logarithmic non-uniformity in the antenna's turns spacing, however, the axial ratio performance is remarkably enhanced, as can be seen from Table 2, which compares average values of axial ratio. Data on the table reveal that the best AR averages occur for the size of ground plane defined by $\gamma = 3.5$; the only exception to this being the case of $\beta = 0.10, \gamma = 6$.

A number of other interesting features are discernible from the profiles of Figure 4. For example, when the ground plane size is defined by $\gamma = 4.0$, axial ratio, for all values of β has a unique profile over the frequency range ; and in the particular case of the uniform helix, represents the only finite ground plane size, for which axial ratio is greater than 3dB at any frequency.

Table 2. Comparison of average values of axial ratio

Ground Plane Size	$\beta = 0.00$	$\beta = 0.03$	$\beta = 0.05$	$\beta = 0.10$
	AR_{ave} (dB)	AR_{ave} (dB)	AR_{ave} (dB)	AR_{ave} (dB)
Infinite	2.1615	2.0157	1.9645	2.2494
$\gamma = 3.0$	1.4708	0.7800	0.6123	0.4567
$\gamma = 3.5$	1.4331	0.7438	0.5863	0.4492
$\gamma = 4.0$	1.7477	0.9575	0.7766	0.5800
$\gamma = 4.5$	1.5631	0.8208	0.6623	0.4831
$\gamma = 5.0$	1.5923	0.9269	0.8023	1.2240
$\gamma = 6.0$	1.6900	1.0908	0.9598	0.8290

Another interesting feature is that the 3dB axial ratio bandwidth is practically the same (the best possible for the frequency range considered) for the various combinations of γ and β, the cases of the infinite ground plane and $\gamma = 4$ (for the uniformly-wound helix) being exceptions.

3.2. Power gain

The power gain profiles of Figure 5 derive from the computational results obtained with the use of the expression given as **[23]**

$$G_p(dB) = 10\log_{10}\left[\frac{\left(\left|E_\theta(\theta_f,\varphi_f)\right|^2+\left|E_\varphi(\theta_f,\varphi_f)\right|^2\right)}{30\left|I_{in}\right|^2 R_{in}}\right], \qquad (11)$$

where I_{in} and R_{in} feed-point current and feed point input resistance, respectively; while $(\vartheta_f,\varphi_f)=(0^0,0^0)$.

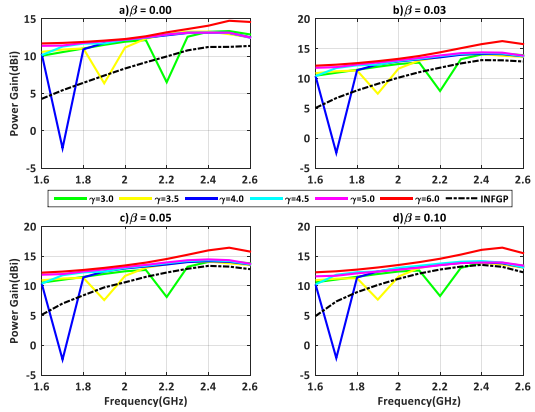

Figure 5.1 Power gain profiles for different sizes of ground plane for various values of β

The curves of Figure 5.1 very clearly show that for all degrees of logarithmic non-uniformity, the use of a ground plane of finite extent, in general significantly improves the power gain response of the antenna. As a matter of fact, maximum achievable gain is consistently higher for the finite ground plane cases than for the large (essentially infinite) ground plane case, as can be seen from Table 3.

Table 3. Maximum achievable gain with various ground plane sizes

Ground Plane Size	$\beta = 0.00$	$\beta = 0.03$	$\beta = 0.05$	$\beta = 0.10$
	Max Gain(dBi)	Max Gain(dBi)	Max Gain(dBi)	Max Gain(dBi)
Infinite	11.3770	13.0970	13.3780	13.5500
$\gamma = 3.0$	13.3700	14.1500	14.1000	13.8700
$\gamma = 3.5$	13.3000	14.1300	14.1200	13.9300
$\gamma = 4.0$	13.1200	14.1400	14.1700	14.0200
$\gamma = 4.5$	13.1700	14.2800	14.3300	14.1900
$\gamma = 5.0$	13.1600	14.3900	14.4700	13.9500
$\gamma = 6.0$	14.7500	16.2800	15.9900	16.4500

Nonetheless, the gain profiles identify a particularly noticeable effect of ground plane size on the gain of the loghelix backed by a ground plane of finite extent.

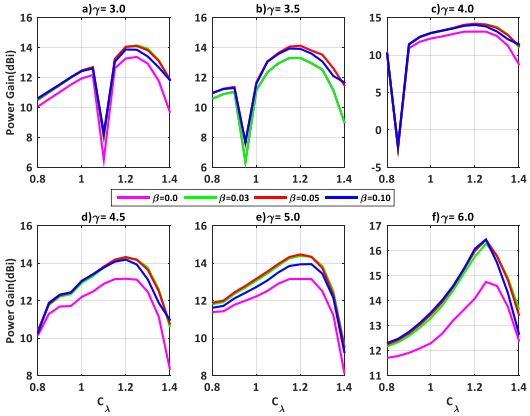

Figure 5.2 Effect of ground plane size on the power gain of the loghelix

In order to underscore this effect, the curves of Figure 5.1 are displayed in the alternative format of Figure 5.2. And as can be seen from the latter set of profiles, power gain is characterized by sharp dips when aspect ratio is less than or equal to 4.0. Because such dips in power gain profiles appear characteristic of antenna structures backed by finite ground planes (see [5] [6], as examples), it is reasonable to conclude that such dips will only feature, when the size of the ground plane relative to the corresponding size of the antenna (or 'aspect ratio'), is less than a critical value. It is worth remarking that in the case of the loghelix under consideration here, the dips associated with power gain coincide with the instances of the 'dominant back lobes identified in section 3.2, as occurring for the relative ground plane sizes defined by $(C_\lambda,\gamma)=(0.85,4.0);(0.95,3.5);(1,10,3.0)$.

3.3. Front-to-back ratio

An antenna radiation pattern's front-to-back ratio represents a measure of the effectiveness of the finite ground plane in reducing backward radiation. It is given by

$$F/B(dB) = 10\log_{10}\left[\frac{\left(\left|E_\theta(\theta_f,\varphi_f)\right|^2+\left|E_\varphi(\theta_f,\varphi_f)\right|^2\right)}{\left(\left|E_\theta(\theta_b,\varphi_b)\right|^2+\left|E_\varphi(\theta_b,\varphi_b)\right|^2\right)}\right] \quad (12)$$

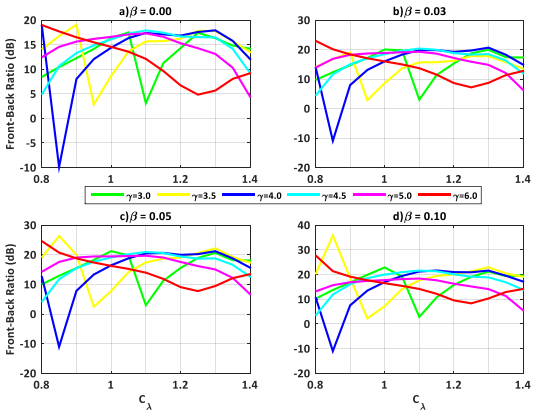

Figure 6.1 Variations of front-to-back ratio with normalized circumference for various combinations of β and γ

In Equation (12), $(\theta_b,\varphi_b)=(180^0,0^0)$, and all other quantities remaining as earlier defined.

Figure 6.1 displays the variations of front-to-back (F/B) ratio with normalized log-helix circumference, for different combinations of geometrical non uniformity and ground plane size. And as may be expected, the dips associated with the power gain profiles also featured in the front-to-back ratio (F/B). Unlike what obtained for power gain and axial ratio (which are pattern 'forward direction' parameters) the F/B ratio curves for all cases of $\gamma = 6$ are markedly different from those for the other values of γ, as can be seen from Figure 6.2. This is evidently due to the fact that F/B ratio, as defined by Equation (12), is function of both main lobe and back lobe parameters.

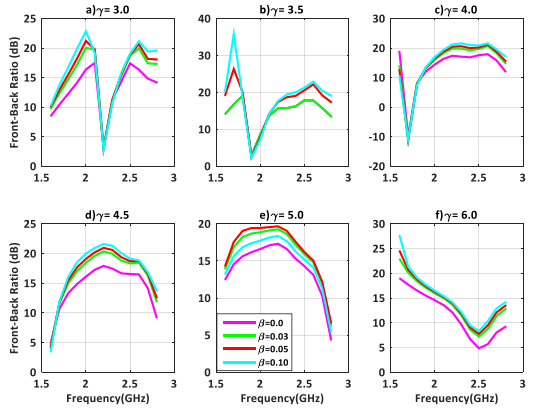

Figure 6.2 Profiles of front-to-back ratio showing influence of ground plane size

4. CONCLUSION

This paper has systematically investigated the influence of ground plane size on the performance characteristics of a helical antenna, whose turns spacing is defined by a logarithmic variation along its axis. Using the structure considered in [**19**] (which examined the effects of the logarithmic non-uniformity) as candidate for the investigations, a Method of Moments analysis involving a wire grid model [6], [8], [**20**], for the circular ground plane was adopted.

Subsequent computational results obtained and comprehensively discussed in the paper reveal a number of interesting features concerning the effects of the ground plane size on the antenna's performance metrics. Notable examples of these include the fact that when the ground plane size, as defined by an aspect ratio denoted by γ is such that $3.0 \le \gamma \le 4.0$, the radiation field pattern is characterized by a 'dominant back lobe', for all degrees of logarithmic non-uniformity. This property is further manifested in the profiles of the antenna's power gain in the forward direction, which, for these values of ground plane size, exhibits what has been described in the paper as sharp 'dips' of the type that feature in the power gain profiles reported in [5], [6], for example. Because the results reveal that these dips are eliminated for ground plane size greater than that defined by $\gamma = 4.0$ in this case, it is concluded that power gain profiles for wire antenna backed by finite-sized ground planes will not exhibit such dips, if the aspect ratio is judiciously specified. This conclusion is, as far as be ascertained, being reported for the first time, in the open literature.

Although similar comments apply for the antenna's axial ratio and F/B profiles, an additional feature emerged in the case of the latter, for γ = 6.0. In this case, F/B ratio generally decreased with C_λ up to about $C_\lambda = 1.25$, when it starts increasing. This suggests that for this ground plane size, radiation field strength is not maximum along the $(0^0,0^0)$ axis in the forward direction, whereas, it is relatively strong along the $(180^0,0^0)$ axis, in the backward direction.

Finally, the computational results very clearly reveal that the use of a finite ground plane significantly enhances the loghelx antenna's performance metrics well beyond the effects of the logarithmic non-uniformity, as reported in [19].

REFERENCES

[1] R. F. Harrington, "Effect of antenna size on gain, bandwidth, and efficiency," *Journal of Research of the National Bureau of Standards,* VOL. 64D(1): Radio Propagation (1960): Pp. 1-12 DOI: https://doi.org/10.6028/JRES.064D.003

[2] A. K. Bhattacharyya, "Effects of finite ground plane on the radiation characteristics of a circular patch antenna," *IEEE Transactions on Antennas and Propagation*, vol. 38, No.. 2, pp. 152-159, Feb. 1990, doi: https://10.1109/8.45116

[3] E. Lier and K. Jakobsen,, "Rectangular microstrip patch antennas with infinite and finite ground plane dimensions," *IEEE Transactions on Antennas and Propagation, vol. 31, No. 6*, pp. 978-984, November 1983, doi: https://10.1109/TAP.1983.1143164

[4] S. Rekha, and M. Nesasudha, "Design of circularly polarized planar monopole antenna with improved axial ratio bandwidth" *Microw Opt Technol Lett*, *Vol 59*, 2017. Pp 2353-2358

[5] H. A. N. Hejase, S. D. Gedney and K. W. Whites, “Effect of a finite ground plane on radiated emissions from a circular loop antenna," *IEEE Transactions on Electromagnetic Compatibility, vol. 36, No. 4*, pp. 364-371, Nov. 1994, doi: https://10.1109/15.328868 .

[6] A. A. Ayorinde, S. A. Adekola, and A. Ike Mowete, “Performance Characteristics of Loop Antennas above a Ground Plane of Finite Extent”, *Progress In Electromagnetics Research Symposium Proceedings,* Taipei, March 25–28, 2013; Pp 769-774.

[7] P. Bolli, M. Bercigli, P. D. Ninni, M. G. Labate and G. Virone, "Preliminary Analysis of the Effects of the Ground Plane on the Element Patterns of SKA1-Low," 2020 14th European Conference on Antennas and Propagation (EuCAP), 2020, pp. 1-5, DOI: https://10.23919/EuCAP48036.2020.9135350 .

[8] D. Basaery; S. M. J. Razavi; S. H. Mohseni Armaki. "Analysis of the Effect of Finite Circular Ground Plane on the Wire Monopole Antennas". *Tabriz Journal of Electrical Engineering*, 47, 1, 2017, 21-28

[9] F. Sadeghkia , M. Mahmoodi , H. Hashemi-Meneh , J. Ghayoomeh, “Helical Antenna Over Different Ground Planes”, *PROC, The 8th European Conference on Antennas and Propagation* (EuCAP 2014*)*, Pp.. 2185 -2188. , DOI: https://10.1109/EuCAP.2014.6902243.

[10] H. Nakano, H. Mimaki and J. Yamauchi, "Numerical analysis of a helical antenna with a finite ground plane," *PROC Antennas and Propagation Society International Symposium, 1986*, pp. 129-132, DOI: https://10.1109/APS.1986.1149805 .

[11] M. Ahmad, M. Amin and A. A. Khan, "Effect of ground plane on the input impedance of Quadrifilar Helix Antenna," *PTOC. 12th International Bhurban Conference on Applied Sciences and Technology (IBCAST),* 2015, pp. 574-578, DOI https://10.1109/IBCAST.2015.7058559

[12] M. Ahmad, A, A. Khan, M. Amin, H. M. Asif, and S. Baig “Ground plane impact on quadrifilar helix antenna performance with respect to deployment heights”, International Journal of Communication Systems, Vol 32(14), September, 2019. Pp. 1-11DOI: https://doi.org/10.1002/dac.40755

[13] S. P. Wadkar, S. M. Rathod, H. Kumar, G. Kumar and B. G. Hogade, "Normal mode helical antenna at 1.8 GHz with small circular ground plane," 2016 International Symposium on Antennas and Propagation (APSYM), 2016, pp. 1-4, DOI: https://10.1109/APSYM.2016.7929145

[14] F. Sadeghikia and A. K. Horestam, "A parametric study on the dimensions of the ground plane of axial-mode helical antennas," 2017 IEEE Asia Pacific Microwave Conference (APMC), 2017, pp. 1127-1129, DOI: https://10.1109/APMC.2017.8251654

[15] I. Egorov and Z. Ying, "A non-uniform helical antenna for dual-band cellular phones," *IEEE Antennas and Propagation Society International Symposium. Transmitting Waves of Progress to the Next Millennium. 2000* Digest. Held in conjunction with: USNC/URSI National Radio Science Meeting (C, 2000, pp. 652-655 vol.2, DOI: https://10.1109/APS.2000.875272

[16] H. M. Elkamchouchi and A. I. Salem, "Helical antennas with nonuniform helix diameter," *Proceedings of the Eighteenth National Radio Science Conference. NRSC'2001 (IEEE Cat. No.01EX462),* 2001, pp. 143-152 vol.1, DOIi: https://10.1109/NRSC.2001.929187

[17] H. M. Elkamchouchi and A. I. A. Salem, "Effects of geometrical parameters, loading, and feeding on nonuniform helical antennas," *Proceedings of the Nineteenth National Radio Science Conference,* 2002, pp. 90-100, DOI: https://10.1109/NRSC.2002.1022610

[18] C. H. Chen, E.K.N. Yung, B. J. Hu, and S.-L. Xie, ” Axial mode helix antenna with exponential spacing” *Microwave and Optical Technology Letters*, Vol 49(7), Pp.1525 - 1530, 2007. https://doi.org/10.1002/mop.22483

[19] A. A. Ayorinde, S. A, Adekola, and A. Ike Mowete, “Logarithmically-Wound Helix Antenna Excited for Axial-Mode Operations”, *Jordan Journal of Electrical Engineering*, Vol. 7(3), September 2021. Pp. 265-287, DOI: https://10.5455/jjee.204-1614026886

[20] D. S. Jones, “Numerical Methods for Antenna problems”, *Proceedings of the Institution of Electrical Engineers,* Vol. 121(7*),* July 1974. Pp. 573-582. DOI: https://doi.org/10.1049/PIEE.1974.0136

[21] R.F. Harrington, 1968, *Field computation by moment methods*, The McMillian Book Company, New York, 1968.

[22] S.X. Ta and T.K. Nguyen, ‘AR bandwidth and gain enhancements of patch antenna using single dielectric superstrate”, *Electronics Letters* Vol.53 (4), July 2017. Pp. 1015-1017 DO!: https://doi.org/10.1049/el.2017.1676

[23] W. Stutzman, G. Thiele, *Antenna theory and design,*: John Wiley, New York, 1981.